Engineering Structures 292 (2023) 116469

Contents lists available at ScienceDirect

Engineering Structures

journal homepage: www.elsevier.com/locate/engstruct

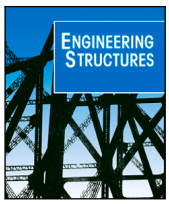

An analytical approach to model Structure–Soil–Structure Interaction (SSSI) of arbitrarily distributed buildings under SH waves

Zubair Zahoor Banday, Xingbo Pu *, Alessandro Marzani, Antonio Palermo *

Department of Civil, Chemical, Environmental and Materials Engineering, University of Bologna, 40136 Bologna, Italy

ARTICLE INFO

Keywords:
Structure–soil–structure interaction
Multiple scattering
Shear horizontal waves
Green's function
Coupled response

ABSTRACT

In this work, a simplified analytical framework based on the multiple scattering theory is proposed to model the structure–soil–structure interaction of buildings excited by antiplane shear waves. To this purpose, each building is modelled as a single degree-of-freedom oscillator, whereas the soil as a viscoelastic layer laying on an elastic half-space. By neglecting the soil-foundation kinematic interaction and considering only its inertial counterpart, the coupled response of buildings is modelled using a multiple scattering approach, where the buildings scattered wavefields are described via Green's functions.

The developed analytical framework is exploited to discuss the dynamic response of a single building, evaluating the variation of its amplitude with respect to the characteristic site frequencies. The dynamics of two buildings are then studied by modelling their coupled response. In particular, the interaction between them is investigated as a function of the buildings spacing, mass, and relative stiffness. Finally, the analysis is extended to the coupled response of a cluster of five buildings. Through the discussed examples, it is demonstrated how the proposed methodology can serve as a computationally inexpensive tool for predicting the interaction among vibrating structures under shear antiplane waves propagating at different frequencies.

1. Introduction

During a seismic event, the ground motion excites all structures to some varying degree. The structures, vibrating, act as additional sources of waves which are radiated back into the soil in the form of scattered wavefields. In urban areas, these scattered wavefields interact with other structures resulting in either amplification or deamplification of the buildings vibrations. In literature, this phenomenon is mainly known as structure–soil–structure interaction (SSSI) [1–3]. The SSSI phenomenon is of importance as it can amplify or diminish the building motion by tens of percent [4].

The study of the interaction between buildings was preceded by the study of the interaction between the foundation of a building and the soil, referred to as soil–structure interaction (SSI) [5,6]. Research into this subject has revealed that the dynamic response of a structure built on a rigid substrate differs notably from the response of an identical structure constructed on flexible support like soft soil [7,8]. The variation in the response is mainly due to the resonance of elastic waves in the flexible substrate which depends on the ratio between the thickness of the layer and the wavelength of the waves [9,10]. In the presence of multiple buildings in the vicinity of each other, this interaction evolves into a cross-interaction problem between the structures, generally referred to as (i) structure–soil–structure interaction (SSSI) [1], (ii) dynamic cross interaction (DCI) [11], or (iii) foundation–soil–foundation interaction (FSFI) [12].

From a historical perspective, studies on how multi-structure systems interact through soil began in the latter half of the 20th century. For an in-depth literature review of SSSI, the reader is referred to [13]. Given the constant increase in computational resources, researchers have rapidly adopted numerical techniques to model complex SSSI configurations, e.g. with multiple different and closely spaced buildings, which were out of the modelling capabilities of the available analytical formulations. In particular, the use of finite element (FE) [14,15], boundary element (BE) [9,10], and coupled FE/BE [16–18] techniques have been proposed. Besides their potential, numerical models remain computationally expensive, can suffer from mesh dependency issues, and can require artificial boundary conditions, like Perfectly Matched Layers (PMLs) for the FEM, to truncate the computational domain [16,19,20]. These aspects render these methods unpractical for parametric analysis and inaccessible to the majority of professionals interested in assessing the effect of SSSI.

In this regard, analytical approaches are desirable since they are able to overcome some of the above limitations while still providing

* Corresponding authors.
E-mail addresses: xingbo.pu2@unibo.it (X. Pu), antonio.palermo6@unibo.it (A. Palermo).

https://doi.org/10.1016/j.engstruct.2023.116469
Received 29 November 2022; Received in revised form 21 April 2023; Accepted 9 June 2023
Available online 30 June 2023

meaningful insights into the SSSI problem. Note that the use of analytical approaches for SSSI modelling trace back to the seminal work of Luco and Contesse [1], who modelled the steady-state response of two parallel shear walls with semi-circular foundations welded to a homogeneous elastic half-space and excited by vertically incident shear horizontal (SH) waves. This work was later extended to investigate the response of multiple shear walls [21,22]. Following a complementary approach, lumped models were later proposed to study structure–soil–structure interactions involving two [23,24] and three buildings [3,25]. Nonetheless, the modelling of multiple buildings interacting in a city-like environment requires the use of a continuous description of the soil substrate where the scattered waves can propagate and interact. In this context, Boutin and Roussillon [26,27] proposed a city-impedance model (CIM) to assess the SSSI effect of the urban environment on seismic motions. In their model, the substrate is described as a homogeneous elastic half-space while the buildings are modelled as a periodic array of equivalent single-degree-of-freedom (SDOF) oscillators. Note that such a SDOF model of the building neglects the soil–structure kinematic interaction and accounts only for its inertial contribution [26]. Indeed, this is a reasonable assumption for buildings lying on thin and rigid foundations [26,27]. Indeed, such a city-impedance model can explain the main features and parameters driving the so-called site–city interactions [28] as demonstrated by comparison with numerical and experimental evidence.

Within the same context, an analytical formulation is proposed here to describe the SSSI problem for incident SH waves, allowing to consider a finite set of different buildings arbitrarily arranged on the soil surface. The formulation exploits a multiple scattering scheme to couple the free incident field with the multiple scattered fields generated by the buildings so to compute their dynamic response and the wave motion within the substrate. In particular, the incident wavefield, generated by shear horizontal waves, is computed at the free surface. The scattered wavefields, radiated in the soil by the buildings, are calculated by means of ad-hoc Green's functions and buildings transfer functions. The latter are derived by describing the buildings as single degree-of-freedom mechanical oscillators.

Compared with most of the available analytical tools, our approach provides some advantages. First, by leveraging the multiple scattering theory to set a mutual wave interaction problem, it allows us to directly obtain the scattered waves generated by each building. Second, it has no constraint on the number of buildings and spacing, in contrast with the city-impedance model of Refs. [26,27] which assumes a regular-infinite arrangement of buildings. This could be particularly attractive for the analyses of soil-city response in irregular urbanized scenarios. Third, it can be easily extended to study the SSSI problem for other mechanical waves such as Rayleigh, Love, and shear vertical (SV) waves.

The work is organized as follows: in Section 2, the proposed analytical framework is detailed. Section 3 presents a series of case studies where single, double and multiple-building scenarios are analysed. In Section 4, some concluding remarks and outlooks on the possible extension of the method are provided.

2. Mathematical framework

In this section, the analytical formulation proposed to model the structure–soil–structure interaction (SSSI) under the action of plane SH waves is described. A schematic of the problem is shown in Fig. 1. In particular, the soil is modelled as a bi-layer medium with a soft soil layer of thickness h laying over the bedrock (Fig. 1a). Structures placed atop the soil are modelled as one-dimensional mechanical resonators, oscillating in the z-direction (Fig. 1b). A generic distribution of N resonators placed at positions x_i, collected in the set $S = \{x_1, x_2, x_3, \dots, x_N | N \in \mathbb{Z}^+\}$, is considered. Harmonic antiplane shear waves polarized in the z direction propagate in the half-space. The resonators, actuated at their bases by the incident SH waves, exert harmonic shear forces at the soil surface which, in turn, radiate additional wavefields (Fig. 1d). The incident and the N radiated, or scattered, wavefields interact such that the dynamic response of each structure depends on the response of the wave-coupled problem [29] (Figs. 1c, d).

To build the related mathematical description, in the following, the formulation of the SH waves free-field displacement (Section 2.1) and the Green's function of the wavefield generated by a surface shear source are recalled (Section 2.2). The free-field and the Green's function are then coupled to the resonators transfer function (Section 2.3) to set up a multiple scattering problem and to obtain the coupled response of SH waves and resonators scattered wavefields (Section 2.4).

2.1. Free-field sh motion for a bi-layer medium

Referring to Fig. 1c, the SH wave field in each layer comprises both up-going ($y > 0$) and down-going ($y < 0$) waves. Following the classical approach for SH waves in layered media [30], a local coordinate system for each layer is defined, and the origins of y axes are set at the top of the bedrock and the soil layer. Accordingly, the corresponding coordinate systems are used to express the scalar wavefield displacements as:

$$w_m = (A_m e^{-i\beta_m y_m} + B_m e^{i\beta_m y_m}) e^{-ik_x x + i\omega t}, \quad m = (L, R) \tag{1}$$

where w_m is the antiplane displacement in z direction. The index m is used to identify the soil layer (L) and the bedrock (R), respectively. In Eq. (1), A_m and B_m are the amplitudes of up-going and down-going plane waves, respectively; k_x and β_m denote the horizontal and vertical wave numbers in layer m, respectively, which satisfy:

$$k_x = \frac{\omega}{C_{s,m}} \cos \vartheta_m, \tag{2a}$$

$$\beta_m = \frac{\omega}{C_{s,m}} \sin \vartheta_m, \tag{2b}$$

where $C_{s,m} = \sqrt{\mu_m / \rho_m}$ refers to the shear wave velocities in the two layers, μ_m and ρ_m denote the shear moduli and the densities of the layers, and ϑ_m is the incidence angle of the SH wavefront (see Fig. 1). It is worth mentioning that material damping can be taken into account in Eqs. (2a), (2b) by introducing complex material properties [31], e.g., the complex shear modulus, as used later in Section 3.

By imposing stress-free boundary condition at $y_L = 0$ and continuity of displacement and stress at the interface ($y_L = -h$), the wave amplitudes A_L, B_L and B_R can be expressed as function of the up-going bedrock amplitude A_R as:

$$A_L = B_L = \frac{1}{\cos \beta_L h + i\bar{\chi} \sin \beta_L h} A_R, \tag{3}$$

$$B_R = \frac{\cos \beta_L h - i\bar{\chi} \sin \beta_L h}{\cos \beta_L h + i\bar{\chi} \sin \beta_L h} A_R, \tag{4}$$

in which $\bar{\chi}$ defines the impedance ratio between the two layers:

$$\bar{\chi} = \frac{\rho_L C_{s,L} \sin \vartheta_L}{\rho_R C_{s,R} \sin \vartheta_R}. \tag{5}$$

2.2. Green's functions for a SH source

The governing scalar wave equations for the two layers read:

$$\nabla^2 w = \frac{1}{C_{s,m}^2} \frac{\partial^2 w(x, y, t)}{\partial t^2}, \quad m = (L, R). \tag{6}$$

Substituting the steady state displacement $w(x, y, t) = w(x, y) e^{i\omega t}$ in Eq. (6), leads to:

$$(\nabla^2 + k_{s,m}^2) w(x, y) = 0, \tag{7}$$

where $\nabla^2 = \frac{\partial^2}{\partial x^2} + \frac{\partial^2}{\partial y^2}$, $k_{s,m} = \frac{\omega}{C_{s,m}}$ is the wavenumber in the domain $m = (L, R)$.

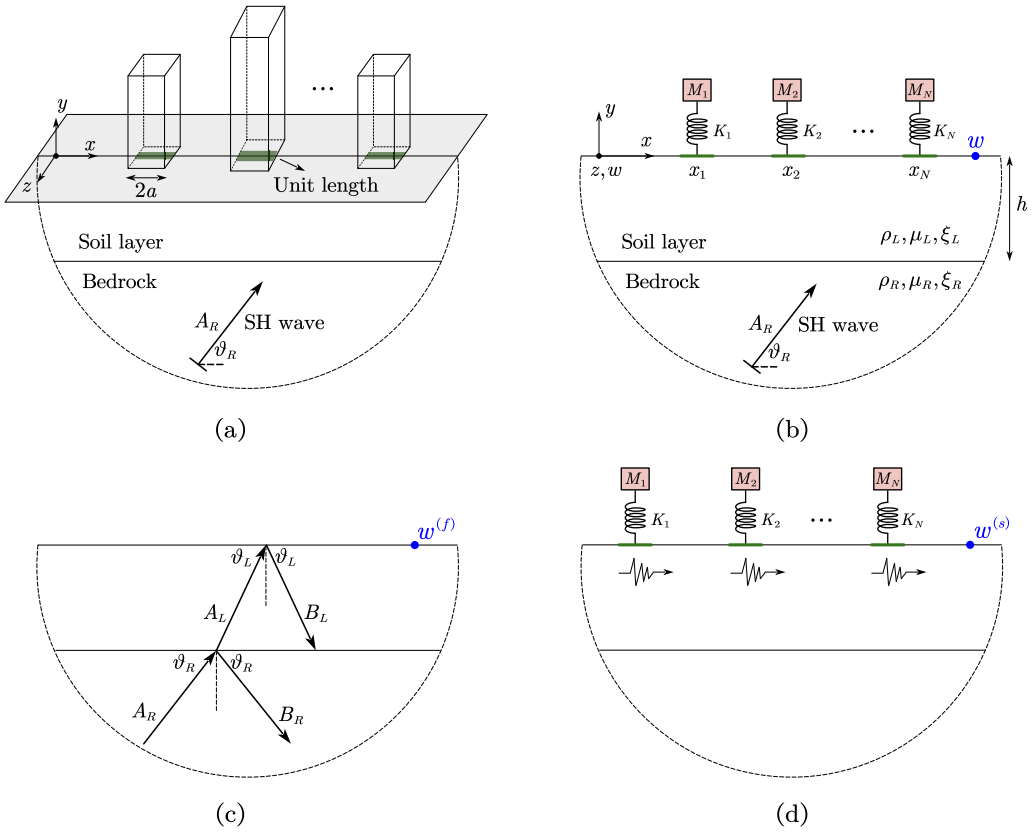

Fig. 1. Schematic of structure–soil–structure interaction for arbitrary configuration of N buildings in a layered half-space. (a) Schematic of buildings. (b) Schematic of the coupled simplified model. (c) Schematic of the free field. (d) Schematic of the scattered fields.

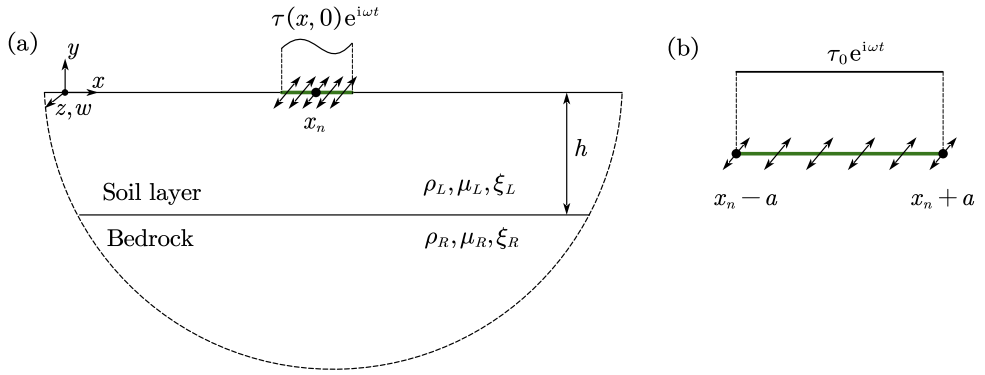

Fig. 2. (a) Schematic of a SH source at the surface of a layered half-space.(b) Detail on a constant, finite length shear source.

The spatial Fourier transform of Eq. (7) along the x axis reads:

$$\left(\frac{\partial^2}{\partial y^2} - q_m^2\right)\tilde{w}(k,y) = 0, \quad m = (L,R) \tag{8}$$

with:

$$\tilde{w}(k,y) = \int_{-\infty}^{\infty} w(x,y)\mathrm{e}^{-\mathrm{i}kx}\,\mathrm{d}x, \tag{9}$$

and $q_m^2 = k^2 - k_{s,m}^2$. The solution of Eq. (8) for the layer ($m = L$) can be written as:

$$\tilde{w}(k,y) = A_1\mathrm{e}^{-q_L y_L} + B_1\mathrm{e}^{q_L y_L}, \quad (-h \le y_L \le 0) \tag{10a}$$

$$\tilde{w}(k,y) = A_2\mathrm{e}^{-q_R y_R} + B_2\mathrm{e}^{q_R y_R} = B_2\mathrm{e}^{q_R y_R}, \quad (y_R \le -h) \tag{10b}$$

where A_2 must vanish to prevent an unbounded response for the bedrock ($m = R$).

At this stage, the computation of the unknown amplitudes in Eqs. (10a), (10b) is performed by imposing stress boundary condition at the half-space surface ($y_L = 0$), continuity of stresses and compatibility of displacements at the interface between the soil layer and the bedrock ($y_L = -h$).

As such, according to Hooke's law, and using the spatial Fourier transform along the x direction, the transformed shear stress in both the domain m can be written as:

$$\tilde{\tau}_{yz}(k,y) = \mu_m \frac{\partial \tilde{w}(k,y)}{\partial y}. \tag{11}$$

Substituting Eq. (10a) into Eq. (11) leads to the transformed shear stress in the soil layer:

$$\tilde{\tau}_{yz}^{(L)}(k,y) = \mu_L(-A_1 q_L\mathrm{e}^{-q_L y_L} + B_1 q_L\mathrm{e}^{q_L y_L}), \quad (-h \le y_L \le 0) \tag{12}$$

Similarly, for the bedrock, the transformed shear stress is calculated by substituting Eq. (10b) into Eq. (11):

$$\tilde{\tau}_{yz}^{(R)}(k,y) = \mu_R q_R B_2 e^{q_R y_R}, \quad (y_R \le -h) \tag{13}$$

The stress boundary condition at the half-space surface ($y_L = 0$) is imposed by equating the layer shear stress of Eq. (11), $\tilde{\tau}_{yz}^{(L)}(k,0)$, to the spatial Fourier transform $\tilde{\tau}_0(k,0)$ of the shear source $\tau_0(x,0)e^{i\omega t}$ acting at the surface, as:

$$\mu_L(-A_1 q_L + B_1 q_L) = \tilde{\tau}_0(k,0), \tag{14}$$

where $\tau_0(x,0)e^{i\omega t}$ is the uniform time-harmonic antiplane shear stress applied at the half-space surface over the resonator base of length $2a$, as illustrated in Fig. 2.

Conversely, at the layer-bedrock interface ($y_L = -h$), a rigid, no-slip, connection is assumed which implies the continuity of displacements and stresses, or, equivalently, the continuity of their Fourier transforms:

$$\tilde{w}^{(L)}(k,-h) = \tilde{w}^{(R)}(k,-h), \tag{15a}$$

$$\tilde{\tau}_{yz}^{(L)}(k,-h) = \tilde{\tau}_{yz}^{(R)}(k,-h). \tag{15b}$$

Substituting Eqs. (10a) and (10b) in Eq. (15) yields:

$$A_1 e^{q_L h} + B_1 e^{-q_L h} = B_2 e^{-q_R h}, \tag{16a}$$

$$\mu_L q_L(-A_1 e^{q_L h} + B_1 e^{-q_L h}) = \mu_R q_R B_2 e^{-q_R h}. \tag{16b}$$

The system of Eqs. (14), (16a), (16b) can be solved as function of the shear stress amplitude $\tilde{\tau}_0$ to obtain:

$$A_1 = \frac{(\mu_L q_L - \mu_R q_R)\,\tilde{\tau}_0}{\mu_L q_L(-\mu_L q_L + \mu_R q_R + \mu_L q_L e^{2hq_L} + \mu_R q_R e^{2hq_L})}, \tag{17a}$$

$$B_1 = \frac{(\mu_L q_L + \mu_R q_R)e^{2hq_L}\,\tilde{\tau}_0}{\mu_L q_L(-\mu_L q_L + \mu_R q_R + \mu_L q_L e^{2hq_L} + \mu_R q_R e^{2hq_L})}, \tag{17b}$$

$$B_2 = \frac{2e^{(q_L+q_R)h}\,\tilde{\tau}_0}{-\mu_L q_L + \mu_R q_R + \mu_L q_L e^{2hq_L} + \mu_R q_R e^{2hq_L}}. \tag{17c}$$

At this stage, by using the inverse Fourier transform, the wavefields in both the soil layer and bedrock are computed as:

$$\mathscr{F}^{-1}[w(k,y)] = w(x,y) = \frac{1}{2\pi}\int_{-\infty}^{\infty}(A_1 e^{-q_L y_L} + B_1 e^{q_L y_L})e^{ikx}\,dk, \quad (-h \le y_L \le 0) \tag{18}$$

$$\mathscr{F}^{-1}[w(k,y)] = w(x,y) = \frac{1}{2\pi}\int_{-\infty}^{\infty} B_2 e^{q_R y_R + ikx}\,dk, \quad (y_R \le -h) \tag{19}$$

2.2.1. Green's function for a unit amplitude, finite length, shear source

Let us assume a rigid, massless, resonator foundation. Under this assumption, the expressions in Eqs. (18) and (19) should be specialized for a harmonic shear stress with constant unit amplitude distributed along a finite length of the half-space surface $[x_n - a, x_n + a]$, as shown in Fig. 2b:

$$\tau_0(x_n,0) = \begin{cases} 1, & \text{if } |x - x_n| \le a \\ 0, & \text{elsewhere} \end{cases} \tag{20}$$

The Fourier transform of Eq. (20) along the x direction reads:

$$\tilde{\tau}_0(k,0) = \frac{2\sin(ka)}{k}e^{-ikx_n}. \tag{21}$$

The Green's function of the wavefields generated by a unitary strip surface shear load is thus obtained by substituting Eq. (21) in Eqs. (17a), (17b), (17c) and combining the results with Eqs. (18) and (19).

2.3. Transmissibility of surface oscillators

Let us consider the dynamic response of the nth oscillator, belonging to the array S, placed on the free surface of the bi-layer medium and excited by a harmonic base motion. As stated in the above section, each oscillator has a footprint length equal to $2a$, so that the area of contact between the resonator and the half-space extends from $(x = x_n - a)$ to $(x = x_n + a)$. The equation of motion for the nth oscillator can be written as:

$$M_n\ddot{W}_n + c_n\dot{W}_n + K_n W_n = c_n\dot{w}_n + K_n w_n, \tag{22}$$

where M_n and K_n denote the mass and the stiffness respectively; c_n is viscous damping coefficient; W_n is the absolute displacement of the resonator; w_n refers to the displacement of the resonator footprint.

At steady state, the ratio of the amplitude of the oscillator motion to the base motion is given by the transmissibility T_n [32]:

$$\frac{W_n}{w_n} \equiv T_n = \frac{\omega_n^2 + 2i\zeta_n\omega_n\omega}{(\omega_n^2 - \omega^2) + 2i\zeta_n\omega_n\omega}, \tag{23}$$

where the resonant angular frequency of the nth oscillator is given by $\omega_n = \sqrt{K_n/M_n}$, while $\zeta_n = c_n/(2M_n\omega_n)$ denotes its damping ratio.

Assuming that the SH wavelength is much greater than the width of the building foundation [33], the small variation of displacement along the foundation is neglected. Thus, for a building/resonator with footprint coordinates $(x_n - a, x_n + a)$, only the displacement at x_n is considered, so that the tangential force applied by the resonator to the elastic medium can be expressed as:

$$P_n = M_n\omega^2 T_n w(x_n,0), \quad \forall\, x_n \in S \tag{24}$$

where $w(x_n,0)$ denotes the displacement at the midpoint resonator footprint. As a result, the uniform shear stress along the soil-resonator contact area is:

$$Q_n(x,0) = \frac{P_n}{2a} \equiv Z_n w(x_n,0) \quad \text{for } x \in (x_n - a, x_n + a),\ x_n \in S \tag{25}$$

2.4. Multiple scattering formulation

Equipped with appropriate expressions for the uniform shear stress along the soil-resonator contact area, Eq. (25), and the related Green's function, Eqs. (18) and (19), a multiple scattering formulation is used to compute the total wavefield within the bi-layered medium. Indeed, when the incident field impinges on the array of N oscillators, the total wave field w can be expressed as the summation of the incident and scattered wave fields [34]:

$$w(x,y) = w^{(f)}(x,y) + \sum_{n=1}^{N} Q_n G_w(x - x_n, y), \tag{26}$$

where $w^{(f)}$ is the incident fields; Q_n is the amplitude of the uniform shear stress at the base of the nth resonator; G_w is the Green's function. At this stage, the stress amplitude Q_n is obtained by substituting Eq. (25) into Eq. (26) and specifying the total displacement at the base of the resonator at position x_m as:

$$Z_m^{-1} Q_m = w^{(f)}(x_m,0) + \sum_{n=1}^{N} Q_n G_w(x_m - x_n, 0), \quad n,m = 1,\dots,N \tag{27}$$

Eq. (27), after some algebra, can be organized in matrix form as [35]:

$$\mathbf{AX} = \mathbf{B}, \tag{28}$$

where:

$$\mathbf{A} = \begin{bmatrix} Z_1^{-1} - G_w(0,0) & -G_w(x_1 - x_2,0) & \cdots & -G_w(x_1 - x_N,0) \\ -G_w(x_2 - x_1,0) & Z_2^{-1} - G_w(0,0) & \cdots & -G_w(x_2 - x_N,0) \\ \vdots & \vdots & \ddots & \vdots \\ -G_w(x_N - x_1,0) & -G_w(x_N - x_2,0) & \cdots & Z_N^{-1} - G_w(0,0) \end{bmatrix},$$

Table 1
Physical parameters and mechanical properties of the substrate and the buildings.

Parameter	Value
Mass density of bedrock, ρ_R	2000 kg/m^3
Mass density of soil layer, ρ_L	1700 kg/m^3
Shear wave velocity of bedrock, $C_{s,R}$	1000 m/s
Shear wave velocity of soil layer, $C_{s,L}$	300 m/s
Depth of soil layer, h	50 m
Hysteretic damping ratio of the soil layer, ξ_L	2%
Hysteretic damping ratio of the bedrock, ξ_R	2%
Unit mass of the building, M	10^5 kg/m
Width of the foundation, $2a$	10 m
Damping ratio of the building, ζ	5%
Layer resonant frequency, f_{s1}	1.5 Hz

$$\mathbf{X} = \begin{bmatrix} Q_1 \\ Q_2 \\ \vdots \\ Q_N \end{bmatrix}, \quad \mathbf{B} = \begin{bmatrix} w^{(f)}(x_1, 0) \\ w^{(f)}(x_2, 0) \\ \vdots \\ w^{(f)}(x_N, 0) \end{bmatrix}. \tag{29}$$

The solution of Eq. (28) provides the vector Q_n. Substitution of Q_n in Eq. (26) allows obtaining the total wave field of the coupled problem in the layered half-space. The reader can refer to Appendix for the numerical validation (via FEM) of the approach.

3. Case studies

The dynamic response of a series of buildings excited by SH waves propagating through the substrate is here examined. The investigation begins by computing the response of a single building considering its interaction with the substrate and, hence, the scattered field generated by its vibration. The results of this analysis are used to better interpret the scenarios of multiple buildings placed in the vicinity of each other and highlight the effects induced by the building–soil–building interactions. The building–soil–building analysis starts, instead, from the configurations with two buildings, where a parametric study is performed to evidence the physical parameters driving the interaction. Then, the study is extended by considering an array of five equally spaced buildings as an example of a highly urbanized scenario.

3.1. Soil–structure interaction for a single building scenario

The dynamic response of a single building overlaying a layered soil is computed assuming the physical and mechanical parameters collected in Table 1. The following assumptions are considered:

- to account for wave energy dissipation, hysteretic damping for the soil layer and the bedrock is considered by assuming a dynamic modulus $\mu'_m = \mu_m + i\mu^*_m$, where $\mu^*_m = 2\xi_m\mu_m$ [36,37], where $m = (L, R)$;
- the site resonant condition is referred to as the configuration where the natural frequency of the building f_n matches the first characteristic frequency of the soil-layer f_{s1}. In this regard, the soil-layer transfer function is denoted as T_S, which accounts for the ground motion amplification due to the presence of the soft layer. In particular, from Eq. (3), the transfer function can be written as $T_S = 2A_L/A_R = \frac{2}{\cos\beta_L h + i\tilde{\gamma}\sin\beta_L h}$. For a small damping in the soil, the resonance occurs when $\cos\beta_L h = 0$, i.e., $f_{s1} = C_{s,L}/(4h)$ for a vertically incident field. This results in the upper bound $|T_S|_{max} = 2\rho_R C_{s,R}/(\rho_L C_{s,L})$. Since vertically incident SH waves lead to the maximum building response, oblique incident SH waves will not be investigated.
- the uncoupled response of the building is evaluated by neglecting the contribution of the scattered field. As such, the normalized absolute displacement for the uncoupled case can be computed as $|W/A_R| = |T_S||T_n|$, where W and A_R represent the amplitudes of the building oscillation and of the incident SH wave in the bedrock, respectively, while T_n is the transmissibility of the building, Eq. (23).

The results for a single oscillator are given in Fig. 3. In particular, Figs. 3a and 3b show the displacement at the top of the building for a range of exciting frequencies of the seismic waves normalized with respect to the amplitude of the incident SH waves in the bedrock (A_R). The solid grey lines represent the displacement for the uncoupled scenario, where the building's scattered field is neglected.

Fig. 3a shows that the peak of the normalized displacement for the coupled scenario $|W/A_R|$ is approximately 30% lower than the uncoupled one $|T_S||T_n|$. This can be explained by taking into consideration the energy radiated by the vibrating building into the substrate, commonly referred to as radiation damping. Additionally, the peak response of the building is shifted towards a lower frequency with respect to the natural frequency of the building [38]. The formulation correctly predicts such time period lengthening [39] and its dependence on the mass of the building and on the stiffness of the underlying strata. Fig. 3b shows the amplitude responses like in Fig. 3a but considering a non-resonant site condition characterized by a natural frequency of the building $f_n = 1.5f_{s1}$. One can again notice a reduction in the peak response of the building in comparison to the uncoupled model. Similarly, the peak of the response occurs at a lower frequency with respect to the uncoupled response. Fig. 3c depicts the peak values of the responses considering buildings with a resonant frequency in the range $0.1 \leq f_n/f_{s1} \leq 2$. Again, it is noticed how the uncoupled model overestimates the building responses when compared to the coupled one. Nonetheless, when $f_n < f_{s1}$, small discrepancies are found between the coupled and the uncoupled predictions. In particular, for $f_n \ll f_{s1}$ the building resonance occurs at the frequency when the soil transfer function is minimal $|T_S| = \min(2A_L/A_R) = 2$. Consequently, the maximum building response can be approximated as $\max|W/A_R| = \max|T_R||T_S| \approx 1/\zeta$. Conversely, for $f_n \approx f_{s1}$, the model predicts a reduction in the peak response by $\sim$ 30% in comparison to the uncoupled model.

Fig. 3d displays the amplitude of the scattered field with respect to the free field, namely $|w^{(s)}/w^{(f)}|$. As expected, the amplitude of the scattered wavefield $|w^{(s)}|$ is not negligible for a site resonant condition $f_n = f_{s1}$. In particular, at the foundation level, for the adopted mechanical parameters, the scattered field amplitude accounts approximately for 60% of the free field. Notably, the amplitude decays for a larger distance due to material and geometric damping as shown by the values calculated at $0.1\lambda_n$, λ_n and $2\lambda_n$ from the building, where $\lambda_n = C_{s,L}/f_n$. As expected, the field decays rapidly away from the building with an amplitude reduction of almost 70% within a distance of one wavelength. At longer distances from the building, the waves are attenuated at a slower rate. This can be partially attributed to the two-dimensional setting of our model, which underestimates the geometrical damping at large distances.

Large amplitudes of the scattered wavefield at resonance can result in a deamplification of the total ground motion $w^{(tot)}$ in the building's close vicinity. To better appreciate this phenomenon, Figs. 3e and 3f display the amplitude ratio $|w^{(tot)}/w^{(s)}|$ [40], and the phase difference between scattered and incident free field. Across the resonant condition, the scattered field at the foundation level becomes out-of-phase with respect to the free field (Fig. 3f, red line). This results in destructive interference between scattered and incident waves yielding an overall reduction of the ground motion close to the building (Fig. 3e, red line). At a distance of one wavelength from the building, one can appreciate an amplification of the ground motion at resonance (Fig. 3e, blue line). Indeed, from Fig. 3f (blue line), it is inferred that the two fields are in-phase for $f = f_n$, thus resulting in a constructive interference that amplifies the total ground motion.

With a clear picture of the single building–soil coupled behaviour, let us proceed to investigate the building–soil–building interaction by considering two oscillators placed over the stratified soil.

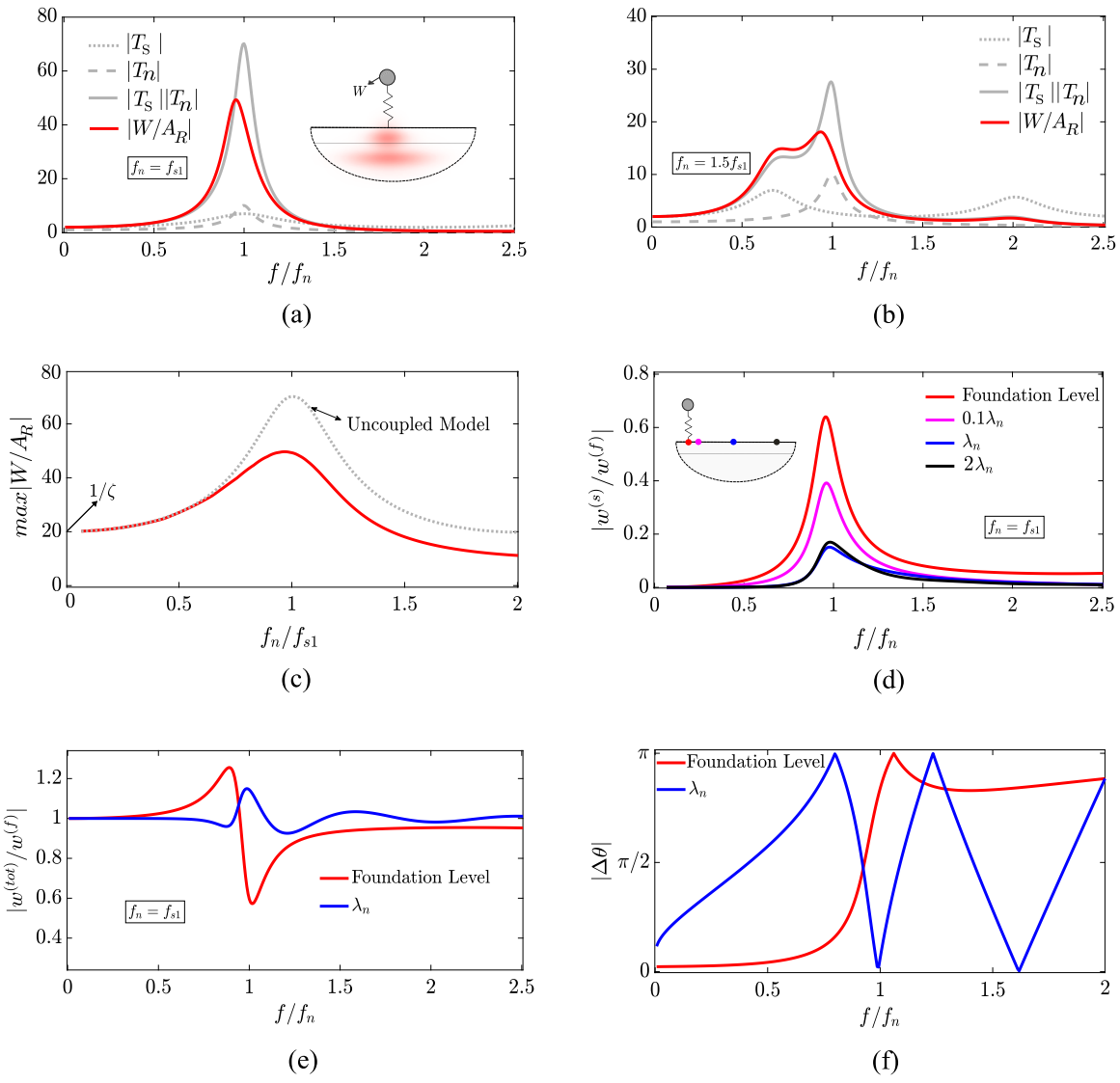

Fig. 3. Dynamic response of a single building coupled to an elastic bi-layer medium in presence of incident SH waves. The normalized building amplitude for (a) site resonant condition ($f_n = f_{s1} = 1.5$ Hz), and (b) non-resonant case ($f_n = 1.5, f_{s1} = 2.25$ Hz). Plot (c) gives the maximum spectral value of the building oscillation. The strength of the scattered field (d), and the total field (e) normalized with respect to the free field have been computed at various distances from the building with $\lambda_n = 200$ m. (f) The phase difference between the free and the scattered field. For comparison, the grey lines represent the uncoupled building response. (For interpretation of the references to colour in this figure legend, the reader is referred to the web version of this article.)

3.2. Building–soil–building interaction

Our investigation starts by considering two buildings placed on top of the elastic bi-layer substrate excited by normally incident SH waves. For all the considered scenarios, the dynamic response of the two buildings are computed assuming the physical and mechanical parameters collected in Table 1, unless otherwise specified. The response of each building is influenced by the total displacement of the soil under their respective foundations.

Fig. 4 reports the results of a configuration consisting of two buildings placed at varying distances from one another. Dashed grey lines denote the coupled response of the building when the other building is not present, here reported to better appreciate the contribution of the building–soil–building interaction.

The interaction between two identical buildings with a natural frequency equal to the first site resonant frequency can either be detrimental or beneficial to the buildings depending on the spacing between them. This can be appreciated from Fig. 4a, where the response of the two identical buildings is reported for different spacing (d=[0.1, 1, 2] λ_n). In particular, a reduction ($\sim$ 20%) of the amplitude of vibration is noted when the buildings are close to each other, e.g., d=0.1λ_n. This beneficial effect is evinced also in Ref. [41], where the SSSI of twin shear walls over a layered half-space is studied via the indirect boundary element method. Conversely, an amplification $\sim$ 10% in the amplitude is registered at the building resonance when the spacing between the buildings is equal to one resonant wavelength λ_n. Again, similar findings are found in Ref. [41].

The structure–soil–structure interaction (SSSI) for two identical buildings having a natural frequency different from the site resonant frequency ($f_n = 1.5 f_s$) shows a similar trend, as evident from Fig. 4b. The SSSI effect is again evidenced at the building resonant frequency ($f = f_{n1}$), while it becomes almost negligible at the soil resonant frequency.

For the case of two non-identical buildings, with building (1) at resonant condition ($f_{n1} = f_{s1}$), the effects of the SSSI are almost imperceptible. This is evidenced by the responses of buildings (1) and (2) reported in Figs. 4c and 4d, respectively. For building (2), which is less stiff than building (1), a marginal amplification/deamplification of amplitude is noted at the resonant frequency of building (1), which, again, depends on the buildings relative distance.

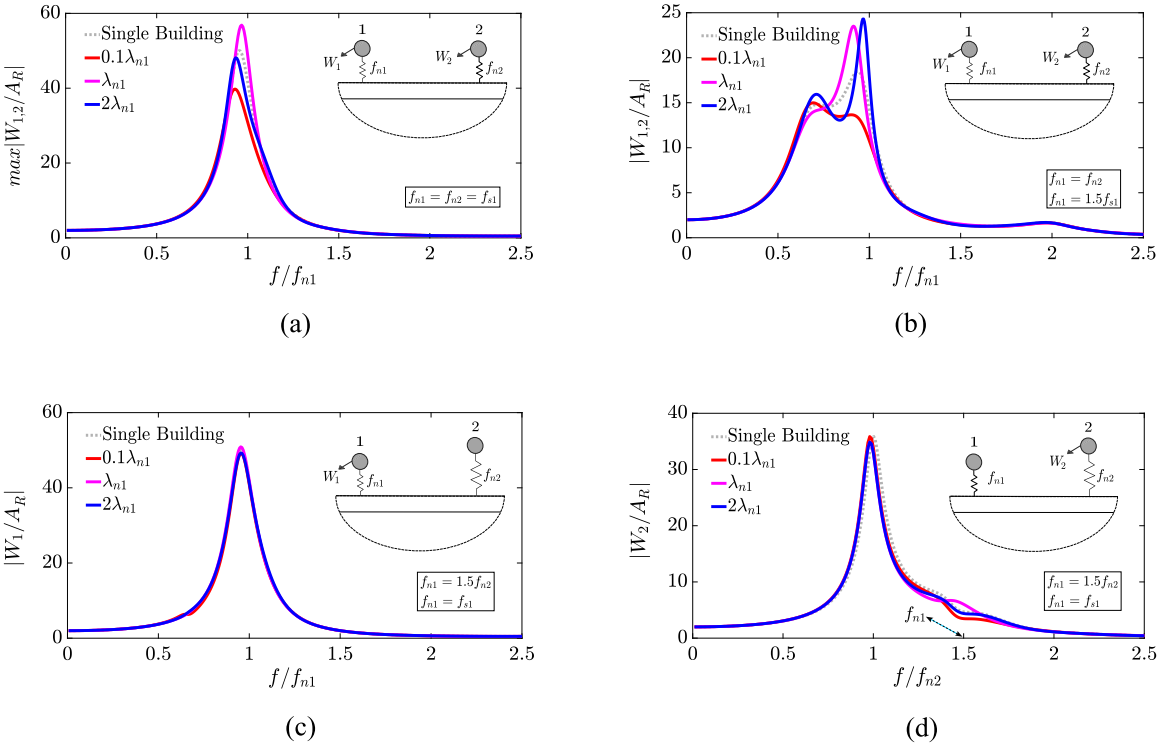

Fig. 4. Effects of building–soil–building interaction. (a) The response of two identical buildings ($f_{n1} = f_{n2} = 1.5$ Hz and $\lambda_{n1} = 200$ m) at site resonant condition. (b) A non-resonant case ($\lambda_{n1} = 133$ m). Similar analysis has been carried out in (c) and (d) for a pair of non-identical buildings with $\lambda_{n1} = 200$ m. Grey plots represent the coupled response of a stand-alone building. (For interpretation of the references to colour in this figure legend, the reader is referred to the web version of this article.)

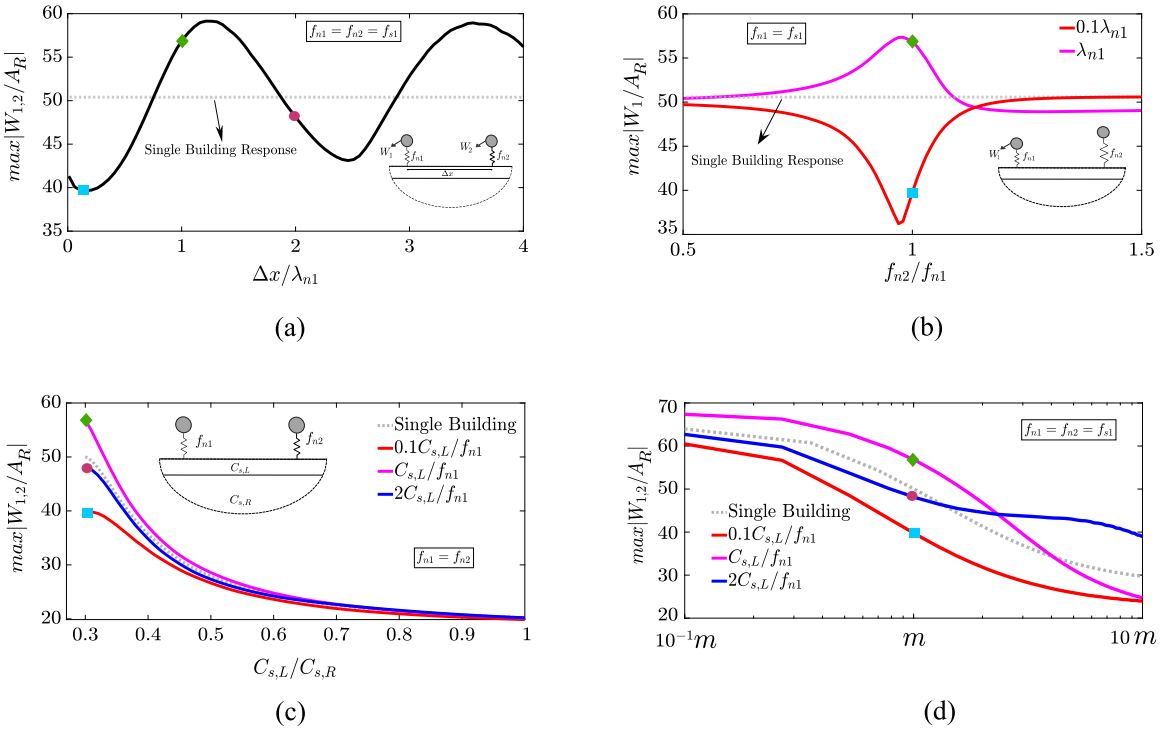

Fig. 5. Coupled response of a pair of buildings with properties chosen from Table 1. Parametric study on (a) spacing between the buildings ($f_{n1} = f_{n2} = f_{s1} = 1.5$ Hz), (b) relative stiffness of the buildings ($\lambda_{n1} = 200$ m), (c) relative stiffness of the soil layer and the bedrock ($f_{n1} = f_{n2} = 1.5$ Hz), and (d) the mass of the buildings ($f_{n1} = f_{n2} = f_{s1} = 1.5$ Hz). Grey plots represent the coupled response of a stand-alone building. (For interpretation of the references to colour in this figure legend, the reader is referred to the web version of this article.)

3.2.1. Parametric study

The SSSI interaction between buildings depends on many parameters, namely the buildings' mass, stiffness, relative distances, etc [42]. In what follows, the sensitivity of this interaction to four major parameters is investigated, namely: the spacing between the buildings, the relative stiffness of the buildings, the mass of the buildings, and the relative stiffness of the soil layer to the bedrock.

Fig. 5a plots the maximum response of two identical buildings as a function of the distance between them. The horizontal grey plot is the response of a stand-alone building. For two buildings placed in the vicinity of each other ($\Delta x < 0.7\lambda_{n1}$), there is a reduction in amplitude in comparison to the single building scenario. Conversely, a maximum amplitude response occurs for a distance $\Delta x \approx 1.1\lambda_n$, consistent with results provided in Ref. [41]. Indeed, the amplification/deamplification of building (1) response with the inter distance Δx follows a clear oscillatory behaviour, with a characteristic length given approximately by $2\lambda_c$, with $\lambda_c = C_{s,L}/f_c$, where f_c is the coupled resonant frequency, namely the resonance frequency of the building (1) lying over the soft layer.

To better appreciate the effect of building distance across the whole frequency range of interest, Fig. 5b compares the maximum response of a single building (1) with its maximum response in presence of building (2) for a range of natural frequency ratio of the two buildings. The study is performed for two building distances, $0.1\lambda_{n1}$ and λ_{n1}. It is observed that the buildings have a negligible effect on each other when their natural periods are well separated. Conversely, one can appreciate the SSSI effect when the two buildings have comparable natural frequencies ($f_{n1} \approx f_{n2}$). A comparison with Fig. 3f helps the reader in understanding the deamplification and amplification of the building's response when placed $0.1\lambda_{n1}$ and λ_{n1} from each other respectively.

The third parameter that has been considered is the relative stiffness of the soil layer to the stiffness of the bedrock. In particular, for every value of the shear wave velocity ratio $C_{s,L}/C_{s,R}$, the maximum displacement of two identical structures is computed. Three building distances of $0.1C_{s,L}/f_{n1}$, $C_{s,L}/f_{n1}$, and $2C_{s,L}/f_{n1}$ are considered, and the response is compared with that of a stand-alone building. As the soil layer becomes more rigid and its shear wave velocity approaches that of the bedrock ($C_{s,L} \sim C_{s,R}$), the SSSI effects become negligible as $|W/A_R| \to 1/\zeta$, see Fig. 5c. This is directly attributed to the diminishing strength of the scattered wavefields in stiff soils and the absence of the amplification of the seismic waves in non-layered substrates [43].

Finally, similar to the scenario in Fig. 5c, two identical buildings are chosen and placed at three different distances from one another while varying the masses of both buildings. The results, in terms of max peak responses, are plotted in Fig. 5d. For low mass structures, all three plots converge to the peak response of the uncoupled model as $|W/A_R| \to |T_S||T_n|$, see Fig. 3a, confirming that the strength of the scattered wavefields is negligible for low mass buildings. Consequently, building–soil–building interactions are insignificant. As the mass increases, the strength of the scattered fields increases. The structures radiate more energy back into the substrate, thus reducing the amplitude of vibrations [44].

3.2.2. An array of buildings

The proposed model is able to treat a generic number of structures. Here, the response of five adjacent buildings with identical dynamic properties is computed and discussed. Two configurations with a constant building spacing of $0.1\lambda_n$ and λ_n are examined at site resonant and non-resonant conditions. The results are shown in Fig. 6. Due to the symmetry of the configurations, the pairs of buildings (1, 5) and (2, 4) have identical responses in the presence of normally incident SH waves.

The case of buildings at site resonance ($f_n = f_{s1}$) with a building spacing of $0.1\lambda_n$ and λ_n are plotted in Figs. 6a and 6b respectively. For a spacing of $0.1\lambda_n$, the peak response of all the buildings in the array is almost halved compared to the single-building scenario. This beneficial group effect is consistent with the findings provided in Ref. [45], where dense arrays of structures interacting with the soil, to model a seismic site–city configuration, are studied using 2D boundary element method. The cause for such behaviour is credited to the reduction of the ground motion in the close vicinity of the buildings at resonance. The buildings are shielded from the seismic waves due to multiple scattered fields cancelling out a fraction of the ground motion at the base of each building. This phenomenon can be thought of as a case of buildings acting as tuned mass dampers (TMDs) by oscillating out-of-phase with the input motion [3]. Similar effects are also evidenced in the so-called seismic metasurfaces, where regular array of resonant units are purposely exploited to dampen out the propagation of seismic waves [46,47]. For spacing of λ_n, the response remains fairly identical to the single building case.

For the non-resonant case ($f_n = 1.5f_{s1}$), the response of the buildings for a spacing of $0.1\lambda_n$ is markedly lower than the stand-alone building, as evident from Fig. 6c. Conversely, for a spacing of λ_n, significant amplification of the building response occurs at the building resonance, Fig. 6d. As the non-resonant case ($f_n \neq f_{s1}$) is more likely to be encountered in a real-world scenario, the detrimental effects of SSSI should be considered when the structures are placed a few hundred meters apart [48].

4. Conclusions

In this work, a simple analytical formulation to study the interaction of buildings during seismic motion has been developed. Buildings are modelled as single degree-of-freedom resonators and SH waves are considered as input ground motions. By exploiting a multiple scattering formulation, the mutual responses of the buildings are coupled through the substrate. The method can capture the effects of the incident and scattered wavefields on the response of the structures. The formulation is able to handle a generic number of structures arranged on the surface of the substrate in a random configuration. The model has been validated for a single building to capture the soil–building interaction before addressing the more complex dynamic interaction of two buildings. For the two building scenarios, a large parametric study has been performed considering:

- The effects of the building distance on the buildings response. Results have evidenced how a pair of closely spaced buildings have a lower dynamic response with respect to a stand-alone building. Furthermore, it has been evidenced and explained the occurrence of response amplification at specific building distances (e.g. $d \approx 1.1\lambda$).
- The effects of the relative building resonant frequencies on the buildings maximum response, quantifying the reduction and the increase for two distinct building spacing ($0.1\lambda_n and \lambda_n$).
- The effects of the relative stiffness between the soil layer/bedrock. Results have evidenced that SSSI effects become less significant when a stiffer soil layer is considered.
- The effects of the relative mass of the buildings at various building distances, showing how SSSI effects become more pronounced when large mass structures are considered.

It is remarked here that the conducted parametric study accounts for a total of more than 600 scenarios. The vast number of considered configurations underlines the suitability of our inexpensive computation tool to perform large parametric analysis and provide a qualitative indication of mechanical parameters driving the SSSI effects for antiplane shear waves.

Finally, the response of a cluster of five closely spaced buildings has been evaluated. For such an array of buildings, the interactions become particularly significant when the site-building resonance occurs, resulting in a collective effect that reduces ground motion throughout the entire building set. This effect can be significant, reducing the building motion by almost 50%.

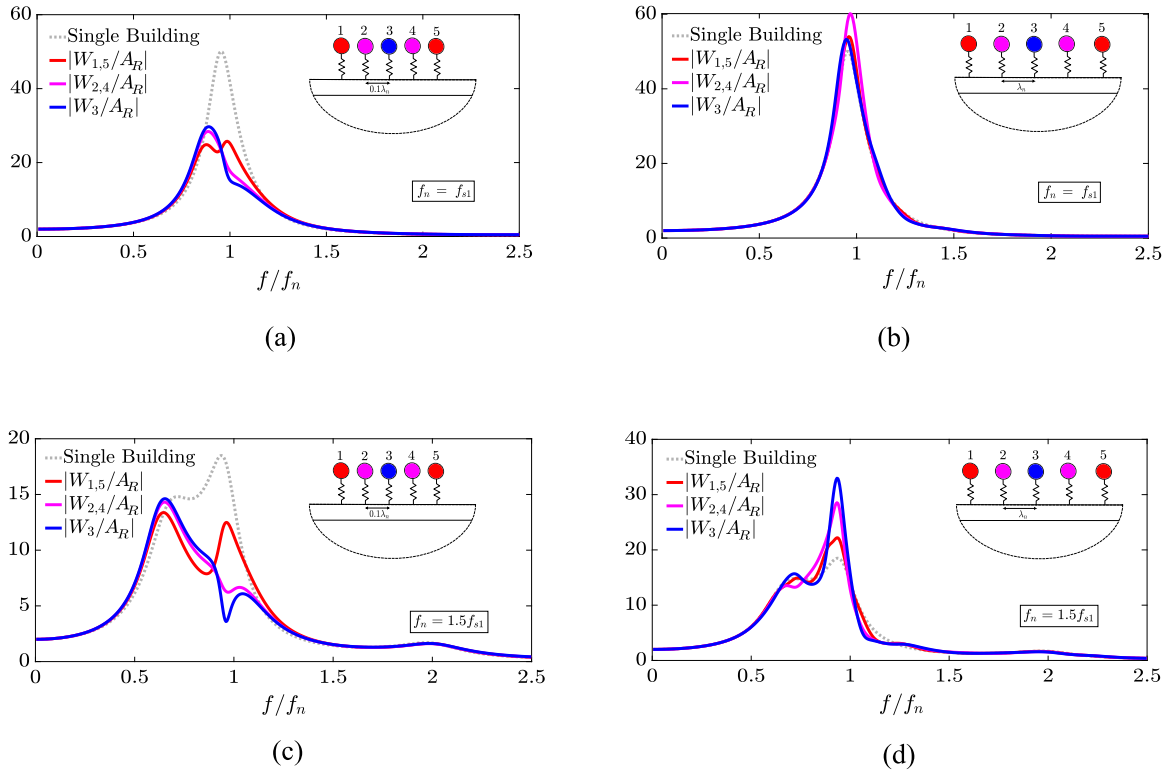

Fig. 6. Response of an array of five equally spaced identical buildings with physical parameters chosen from Table 1. Results are computed for a spacing of $0.1\lambda_n$ and λ_n. Plots (a) and (b) refer to the site resonant case ($\lambda_n = 200$ m) while (c) and (d) exhibit the results for a non-resonant case ($\lambda_n = 133$ m). Grey plots represent the coupled response of a stand-alone building. (For interpretation of the references to colour in this figure legend, the reader is referred to the web version of this article.)

Overall, the proposed simplified model allows to shed light on the period lengthening of structures on soft soils, the mutual interaction between multiple close buildings and the dependence of this interaction on various physical parameters. The model can be used as a computationally inexpensive tool for a preliminary assessment of SSSI. Due to its flexibility, the proposed formulation can be easily extended to deal with SV problems. Note that the free field and Green's function for in-plane shear strip sources on a bilayer half-space are readily available in [49]. Future research efforts will be devoted to extending the methodology to include multiple degree-of-freedom systems coupled to a 3D substrate, thus paving the way to study seismic site–city interaction with simple analytical tools.

CRediT authorship contribution statement

Zubair Zahoor Banday: Investigation, Formal analysis, Writing – original draft. **Xingbo Pu:** Methodology, Investigation, Formal analysis, Validation, Software, Writing – review & editing. **Alessandro Marzani:** Conceptualization, Writing – review & editing, Supervision, Funding acquisition. **Antonio Palermo:** Methodology, Conceptualization, Formal analysis, Software, Writing – review & editing, Supervision.

Declaration of competing interest

The authors declare that they have no known competing financial interests or personal relationships that could have appeared to influence the work reported in this paper.

Data availability

No data was used for the research described in the article.

Acknowledgements

This project has received funding from the European Union's Horizon 2020 research and innovation program under the Marie Skłodowska Curie grant agreement No 813424.

Appendix. Validation of the multiple scattering formulation

In this Appendix, a truncated 3D FE model (soil layer) is built in COMSOL Multiphysics (Fig. A.1a) with dimensions $\ell_x = 800$ m, $\ell_y = h = 50$ m, $\ell_z = 1$ m, to verify the multiple scattering formulation provided in Eq. (28). To capture the mutual interaction, two identical buildings with resonance frequency $f_{n1} = f_{n2} = 1.5 and f_{s1} = 2.25$ Hz are considered, where a centre distance of 200 m ($x_1 = -100$ m, $x_2 = 100$ m) is assumed. To simulate the uniform antiplane SH force imposed on the footprint by each building, the SDOF resonator is modelled by a distribution of $n = 11$ truss elements, in which each point mass is $m_t = M/11$, and the Young's modulus $E_t = (m_t\omega^2 + 2im_t\zeta\omega_n\omega)\ell_t/A_t$, where ℓ_t and A_t denote the length and cross-sectional area of the truss.

To model the antiplane SH wave propagation, the displacement components in the x and y directions are prescribed as $u = 0, v = 0$ in the whole model. Additionally, a pair of continuous boundary conditions, i.e., $w(x, y, z = 0) = w(x, y, z = -\ell_z)$, are imposed on the front and back faces to ensure the antiplane invariance of SH waves in the z direction. It should be noticed that the truncation of the computation domain along the x-axis plays a role in the resonator response. Following Ref. [50], a pair of periodic boundary conditions, i.e., $w(x = -\ell_x/2, y, z) = w(x = \ell_x/2, y, z)$, are imposed on the left and right faces. Although, such an operation is equivalent to analysing an infinitely periodic system, this approximation is reasonable when the model is large enough due to the weak coupling. In our numerical simulations, the convergent result is obtained for $|\ell_x/2 - x_2| > 2\lambda_n$.

To simulate the vertical SH-wave input, the shear stress $f_{yz} = \rho_R C_{s,R}\partial w'/\partial t + \tau'_{yz}$, where the prime denotes a quantity in the free

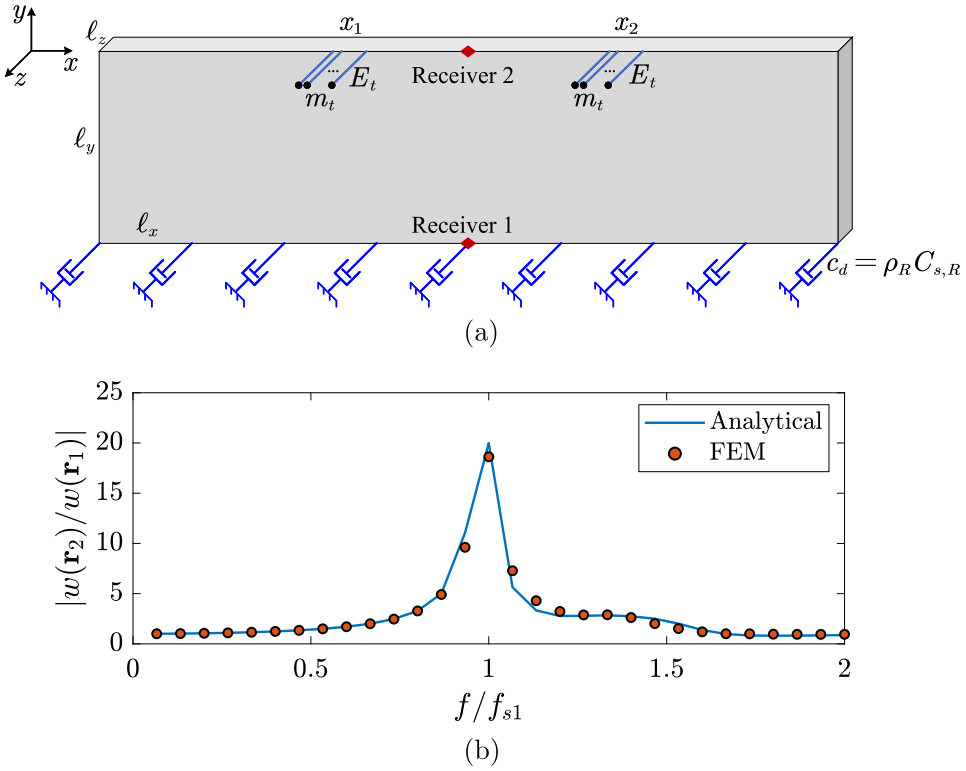

Fig. A.1. (a) Schematic of the 3D FE model. (b) Comparison between the FE and analytical solutions.

field. To absorb outgoing waves, the Lysmer–Kuhlemeyer dashpot [51] is used: $f_{yz} = -c_d \partial w/\partial t = -\rho_R C_{s,R} \partial w/\partial t$.

Using the same parameters displayed in Table 1 and meshing the model using free tetrahedral element, we calculate and show the amplitude ratio vs. frequency in the range of $f = (0, 2]f_{s1}$ in Fig. A.1b at two locations, namely, the receiver 1 at $\mathbf{r}_1 = (0, 0, -h)$ m and receiver 2 at $\mathbf{r}_2 = (0, 0, 0)$ m. The FE simulations, marked by circles, are in good agreement with the analytical results (solid line) computed using Eq. (28).

References

[1] Luco JE, Contesse L. Dynamic structure-soil-structure interaction. Bull Seismol Soc Am 1973;63(4):1289–303. http://dx.doi.org/10.1785/BSSA0630041289.

[2] Wang S, Schmid G. Dynamic structure-soil-structure interaction by FEM and BEM. Comput Mech 1992;9(5):347–57. http://dx.doi.org/10.1007/BF00370014.

[3] Aldaikh H, Alexander NA, Ibraim E, Oddbjornsson O. Two dimensional numerical and experimental models for the study of structure–soil–structure interaction involving three buildings. Comput Struct 2015;150:79–91. http://dx.doi.org/10.1016/j.compstruc.2015.01.003.

[4] Behnamfar F, Sugimura Y. Dynamic response of adjacent structures under spatially variable seismic waves. Probab Eng Mech 1999;14(1–2):33–44. http://dx.doi.org/10.1016/S0266-8920(98)00033-2.

[5] Mylonakis G, Gazetas G. Seismic soil-structure interaction: beneficial or detrimental? J Earthq Eng 2000;4(3):277–301. http://dx.doi.org/10.1080/13632460009350372.

[6] Wolf JP, Song C. Some cornerstones of dynamic soil–structure interaction. Eng Struct 2002;24(1):13–28. http://dx.doi.org/10.1016/S0141-0296(01)00082-7.

[7] Chopra AK, Gutierrez JA. Earthquake response analysis of multistorey buildings including foundation interaction. Earthq Eng Struct Dynam 1974;3(1):65–77. http://dx.doi.org/10.1002/eqe.4290030106.

[8] Bielak J. Modal analysis for building-soil interaction. J Eng Mech Div 1976;102(5):771–86. http://dx.doi.org/10.1061/JMCEA3.0002160.

[9] Liang J, Fu J, Todorovska MI, Trifunac MD. Effects of the site dynamic characteristics on soil–structure interaction (I): Incident SH-waves. Soil Dyn Earthq Eng 2013;44:27–37. http://dx.doi.org/10.1016/j.soildyn.2012.08.013.

[10] Liang J, Fu J, Todorovska MI, Trifunac MD. Effects of site dynamic characteristics on soil–structure interaction (II): Incident P and SV waves. Soil Dyn Earthq Eng 2013;51:58–76. http://dx.doi.org/10.1016/j.soildyn.2013.03.003.

[11] Kitada Y, Hirotani T, Iguchi M. Models test on dynamic structure–structure interaction of nuclear power plant buildings. Nucl Eng Des 1999;192(2–3):205–16. http://dx.doi.org/10.1016/S0029-5493(99)00109-0.

[12] Mulliken J, Karabalis D. Discrete model for foundation-soil-foundation interaction. WIT Trans Built Environ 1970;15. http://dx.doi.org/10.2495/SD950561.

[13] Lou M, Wang H, Chen X, Zhai Y. Structure–soil–structure interaction: Literature review. Soil Dyn Earthq Eng 2011;31(12):1724–31. http://dx.doi.org/10.1016/j.soildyn.2011.07.008.

[14] Bolisetti C, Whittaker AS. Numerical investigations of structure-soil-structure interaction in buildings. Eng Struct 2020;215:110709. http://dx.doi.org/10.1016/j.engstruct.2020.110709.

[15] Long H, Wang Z, Zhang C, Zhuang H, Chen W, Peng C. Nonlinear study on the structure-soil-structure interaction of seismic response among high-rise buildings. Eng Struct 2021;242:112550. http://dx.doi.org/10.1016/j.engstruct.2021.112550.

[16] Rizos D, Wang Z. Coupled BEM–FEM solutions for direct time domain soil–structure interaction analysis. Eng Anal Bound Elem 2002;26(10):877–88. http://dx.doi.org/10.1016/S0955-7997(02)00057-7.

[17] Genes MC, Kocak S. Dynamic soil–structure interaction analysis of layered unbounded media via a coupled finite element/boundary element/scaled boundary finite element model. Internat J Numer Methods Engrg 2005;62(6):798–823. http://dx.doi.org/10.1002/nme.1212.

[18] Padron L, Aznarez J, Maeso O. Dynamic structure–soil–structure interaction between nearby piled buildings under seismic excitation by BEM–FEM model. Soil Dyn Earthq Eng 2009;29(6):1084–96. http://dx.doi.org/10.1016/j.soildyn.2009.01.001.

[19] Romero A, Galvín P, Domínguez J. 3D non-linear time domain FEM–BEM approach to soil–structure interaction problems. Eng Anal Bound Elem 2013;37(3):501–12. http://dx.doi.org/10.1016/j.enganabound.2013.01.001.

[20] Vasilev G, Parvanova S, Dineva P, Wuttke F. Soil-structure interaction using BEM–FEM coupling through ANSYS software package. Soil Dyn Earthq Eng 2015;70:104–17. http://dx.doi.org/10.1016/j.soildyn.2014.12.007.

[21] Wong H, Trifunac M. Two-dimensional, antiplane, building-soil-building interaction for two or more buildings and for incident planet SH waves. Bull Seismol Soc Am 1975;65(6):1863–85. http://dx.doi.org/10.1785/BSSA0650061863.

[22] Murakami H, Luco JE. Seismic response of a periodic array of structures. J Eng Mech Div 1977;103(5):965–77. http://dx.doi.org/10.1061/JMCEA3.0002286.

[23] Vicencio F, Alexander NA. Higher mode seismic structure-soil-structure interaction between adjacent building during earthquakes. Eng Struct 2018;174:322–37. http://dx.doi.org/10.1016/j.engstruct.2018.07.049.

[24] Alexander N, Ibraim E, Aldaikh H. A simple discrete model for interaction of adjacent buildings during earthquakes. Comput Struct 2013;124:1–10. http://dx.doi.org/10.1016/j.compstruc.2012.11.012.
[25] Lu Y, Li B, Xiong F, Ge Q, Zhao P, Liu Y. Simple discrete models for dynamic structure-soil-structure interaction analysis. Eng Struct 2020;206:110188. http://dx.doi.org/10.1016/j.engstruct.2020.110188.
[26] Boutin C, Roussillon P. Assessment of the urbanization effect on seismic response. Bull Seismol Soc Am 2004;94(1):251–68. http://dx.doi.org/10.1785/0120030050.
[27] Boutin C, Roussillon P. Wave propagation in presence of oscillators on the free surface. Internat J Engrg Sci 2006;44(3–4):180–204. http://dx.doi.org/10.1016/j.ijengsci.2005.10.002.
[28] Schwan L, Boutin C, Padrón L, Dietz MS, Bard P-Y, Taylor C. Site-city interaction: Theoretical, numerical and experimental crossed-analysis. Geophys J Int 2016;205(2):1006–31. http://dx.doi.org/10.1093/gji/ggw049.
[29] Pu X, Palermo A, Marzani A. Lamb's problem for a half-space coupled to a generic distribution of oscillators at the surface. Internat J Engrg Sci 2021;168:103547. http://dx.doi.org/10.1016/j.ijengsci.2021.103547.
[30] Haskell NA. Crustal reflection of plane SH waves. J Geophys Res 1960;65(12):4147–50. http://dx.doi.org/10.1029/JZ065i012p04147.
[31] Wolf JP, Obernhuber P. Free-field response from inclined SH-waves and Love-waves. Earthq Eng Struct Dynam 1982;10(6):823–45. http://dx.doi.org/10.1002/eqe.4290100607.
[32] Paz M. Structural dynamics: theory and computation. Springer Science & Business Media; 2012.
[33] Fanchi JR. Principles of applied reservoir simulation. 4th ed.. Elsevier Science; 2018.
[34] Pu X, Palermo A, Marzani A. A multiple scattering formulation for finite-size flexural metasurfaces. Proc R Soc Lond Ser A Math Phys Eng Sci 2022;478(2262):20210669. http://dx.doi.org/10.1098/rspa.2021.0669.
[35] Pu X, Palermo A, Marzani A. Topological edge states of quasiperiodic elastic metasurfaces. Mech Syst Signal Process 2022;181:109478. http://dx.doi.org/10.1016/j.ymssp.2022.109478.
[36] Bert CW. Material damping: An introductory review of mathematic measures and experimental technique. J Sound Vib 1973;29(2):129–53. http://dx.doi.org/10.1016/S0022-460X(73)80131-2.
[37] Presti DCL, Pallara O, Cavallaro A. Damping ratio of soils from laboratory and in situ tests. In: Seismic behaviour of ground and geotechnical structures. CRC Press; 2021, p. 391–400.
[38] Piro A, de Silva F, Parisi F, Scotto di Santolo A, Silvestri F. Effects of soil-foundation-structure interaction on fundamental frequency and radiation damping ratio of historical masonry building sub-structures. Bull Earthq Eng 2020;18(4):1187–212. http://dx.doi.org/10.1007/s10518-019-00748-4.
[39] Veletsos AS, Nair VD. Seismic interaction of structures on hysteretic foundations. J Struct Div 1975;101(1):109–29. http://dx.doi.org/10.1061/JSDEAG.0003962.
[40] Woods RD. Screening of surface wave in soils. J Soil Mech Found Div 1968;951–79. http://dx.doi.org/10.1061/JSFEAQ.0001180.
[41] Liang J, Han B, Todorovska MI, Trifunac MD. 2D dynamic structure-soil-structure interaction for twin buildings in layered half-space I: Incident SH-waves. Soil Dyn Earthq Eng 2017;102:172–94. http://dx.doi.org/10.1016/j.soildyn.2017.08.017.
[42] Bybordiani M, Arici Y. Structure-soil-structure interaction of adjacent buildings subjected to seismic loading. Earthq Eng Struct Dynam 2019;48(7):731–48. http://dx.doi.org/10.1002/eqe.3162.
[43] Semblat J, Pecker A. Waves and vibrations in soils: earthquakes, traffic, shocks, construction works. IUSS Press, Pavia; 2009.
[44] Xiong W, Jiang L-Z, Li Y-Z. Influence of soil–structure interaction (structure-to-soil relative stiffness and mass ratio) on the fundamental period of buildings: Experimental observation and analytical verification. Bull Earthq Eng 2016;14(1):139–60. http://dx.doi.org/10.1007/s10518-015-9814-2.
[45] Kham M, Semblat J-F, Bard P-Y, Dangla P. Seismic site–city interaction: Main governing phenomena through simplified numerical models. Bull Seismol Soc Am 2006;96(5):1934–51. http://dx.doi.org/10.1785/0120050143.
[46] Palermo A, Krödel S, Marzani A, Daraio C. Engineered metabarrier as shield from seismic surface waves. Sci Rep 2016;6(1):1–10. http://dx.doi.org/10.1038/srep39356.
[47] Pu X, Palermo A, Cheng Z, Shi Z, Marzani A. Seismic metasurfaces on porous layered media: Surface resonators and fluid-solid interaction effects on the propagation of Rayleigh waves. Internat J Engrg Sci 2020;154:103347. http://dx.doi.org/10.1016/j.ijengsci.2020.103347.
[48] Jennings PC. Distant motions from a building vibration test. Bull Seismol Soc Am 1970;60(6):2037–43. http://dx.doi.org/10.1785/BSSA0600062037.
[49] Kausel E. Advanced structural dynamics. Cambridge University Press; 2017.
[50] Al Lethawe M, Addouche M, Benchabane S, Laude V, Khelif A. Guidance of surface elastic waves along a linear chain of pillars. AIP Adv 2016;6(12):121708. http://dx.doi.org/10.1063/1.4972552.
[51] Lysmer J, Kuhlemeyer RL. Finite dynamic model for infinite media. J Eng Mech Div 1969;95(4):859–77. http://dx.doi.org/10.1061/JMCEA3.0001144.